

Received 10 August 2023, accepted 4 September 2023, date of publication 7 September 2023,
date of current version 20 September 2023.

Digital Object Identifier 10.1109/ACCESS.2023.3312992

RESEARCH ARTICLE

Optimization and Experimental Validation of Amorphous Alloy High-Speed Asynchronous Motor for Simultaneous Reduction on Core and Copper Losses

JIAHAO ZHANG¹, (Member, IEEE), RONGGAO CUI², YU WEI¹, DEGUI YU¹, SHUNDE XIE¹,
SHITONG FANG¹, AND JUN SHEN¹

¹College of Mechatronics and Control Engineering, Shenzhen University, Shenzhen 518060, China

²Department of Motor Design Business, Weichai New Energy Technology Company Ltd., Weifang 261061, China

Corresponding author: Shitong Fang (stfang@szu.edu.cn)


This work was supported in part by the National Natural Science Foundation of China under Grant 52205114 and Grant 52071217, in part by the Guangdong Basic and Applied Basic Research Foundation under Grant 2023A1515012921, in part by the Excellent Science and Technology Creative Talent Training Program of Shenzhen under Grant RCBS20221008093252089, and in part by the Shenzhen Natural Science Fund through the Stable Support Plan Program under Grant 20220809181431001.

ABSTRACT Amorphous alloy has been proposed to replace silicon steel as the stator core material of high-speed asynchronous motors so as to reduce their core losses. However, it is found that this is at the expense of increasing the copper loss. Therefore, the optimization of amorphous alloy high-speed asynchronous motors is needed to simultaneously reduce their core and copper losses, which is still an open issue. This paper uses an evolutionary algorithm to achieve this and provides the experimental validation. Firstly, the modeling and finite element simulation of the asynchronous motors with the stator core materials as the amorphous alloy and silicon steel are presented and compared. Secondly, with the knowledge of the optimization objectives of the amorphous alloy asynchronous motor, the evolutionary algorithm is proposed to optimize the shapes of its stator and rotor slots. The related mechanisms are discussed based on the electromagnetism. Thirdly, the experimental validation is conducted. Results show that compared with the silicon steel asynchronous motor (Motor-S) and the amorphous alloy asynchronous motor before optimization (Motor-A), the optimized Motor-A (Motor-AO) has the largest high-efficiency range of output torque and operational speed. Specifically, its efficiency at the output torque of 1.5 N·m and the operational speed of 7000 rpm is increased by 4.29% and 7.12% compared with those of Motor-A and Motor-S, respectively. In addition, the temperature distribution shows that the case and rotor temperatures of Motor-AO is the lowest, indicating its superior comprehensive performance.

INDEX TERMS Amorphous alloy, high-speed asynchronous motor, optimization, core loss, copper loss.

I. INTRODUCTION

In recent years, the high-speed motors have been used in a wide range of applications, such as electric vehicles [1], [2], machine tools [3] and medical devices [4]. However, the energy losses of electric motors account for more than half of the world electricity consumption [5], [6]. Specifically,

The associate editor coordinating the review of this manuscript and approving it for publication was Qinfen Lu .

asynchronous motors have become one kind of the widely used motors because of their simple structures, system reliability and relatively low cost [7], [8]. The power consumption of asynchronous motors accounts for about 70% of the total power consumption of electric motors. In fact, the core and copper losses are two kinds of main consumption sources of asynchronous motor, which are especially high when the motor operates at high speed [9], [10]. Whereas the high-speed motor is in great demand in intelligent

robots, high-precision grinding machines, centrifugal machine, etc.

The cores of the high-speed motors developed in recent years are commonly made of silicon steel. Due to its higher coercivity and lower permeability, the silicon steel can produce higher core losses [11], leading to the motor overheating and therefore the short motor life. Therefore, the reduction of stator core losses has become an important research direction in recent years [12], [13]. Sundaria et al. [14] addressed the problem of core losses by improving the manufacturing process of motor stator, and demonstrated that the core losses can be decreased by 23%. Hu et al. [15] used an optimization method of the stator slot shape to reduce the iron core losses by 24.8%. Jahangiri et al. [16] used the method of laser irradiation on the surface of silicon steel sheets, resulting in a 16.8% reduction of core losses at 50 Hz. However, the decrease percentage of core losses by using these methods is still limited. As a result, researchers have used amorphous alloys to replace silicon steels as the motor stator materials to further reduce core losses. This is due to the reason that amorphous alloys have a lower coercivity and higher permeability. Johnson et al. [17] demonstrated that using the amorphous alloys for motor stators could reduce core losses by around 70% compared with silicon steels. Dems and Komezka [18] compared the core losses of silicon steel asynchronous motors with those of amorphous asynchronous motors, and demonstrated an average reduction of 50% in the core losses of amorphous alloy motors for different operating conditions. Chiba et al. [19] applied the amorphous alloys to switched reluctance motors and found that their core losses were 60% lower than those of silicon steel motors at the rated speed. Therefore, the application of amorphous alloys in motors is a promising way to improve their efficiency by reducing the core losses.

Besides the punching process [20] and material [21] design, the optimization of electric motors is of significance to reduce both core and copper losses and increase the efficiency [22]. Already in 1989, Jazdzynski [23] used the quadratic approximation method for optimizing the silicon steel squirrel-cage asynchronous motors. Fetih and Elshewy [24] applied the method of Rosenbrock nonlinear optimization technique for the asynchronous motors to reduce the losses of motor. Liuzzi et al. [25] proposed a controlled random search algorithm method to solve the optimization problem of conflicting objectives including the manufacturing cost, the rated efficiency, the power factor, and the starting current. Yang et al. [26] studied the method of reducing copper losses in motors by optimizing the number and diameter of copper bars in the rotor, thus improving the efficiency of amorphous asynchronous motors. In recent decades, researchers have proposed more advanced optimization methods to increase the optimization accuracy and efficiency. Lei et al. [27] introduced the fractional orders in the finite element model for the analysis of automotive asynchronous motors, and optimized the stiffness and

mass parameters for automotive silicon steel asynchronous motors. Lin [28] proposed the wolf optimization, the Taguchi method, and the finite element analysis for the two-phase multi-objective optimization problem to reduce stator copper and core losses, thus maximizing the energy efficiency. Cunkas [29] provided a method with the concept of fuzzy sets and genetic algorithms to improve both full-load torque and rated efficiency of motors. However, most of the above optimization methods are based on silicon steel motors, and few optimization research has been conducted to improve the performance of amorphous alloy motors [30]. The optimization processes for silicon steel motors are not applicable to amorphous alloy motor design as the properties of amorphous alloys, such as saturation density and permeability, are different from those of conventional silicon steel sheets. Furthermore, it is found in this paper that the design of amorphous alloy stator core reduces the core loss at the expense of increasing the copper loss. The non-crystalline structure of amorphous alloys results in reduced hysteresis and eddy current losses, thereby minimizing iron core heating. However, amorphous alloys have lower saturation magnetic flux density than crystalline materials, implying that to achieve the same magnetic flux density, an increase in current through copper conductors is required. This leads to higher copper losses, which are the thermal losses generated in the copper conductors as current flows through them. Therefore, it is of significance to present the optimization and analysis methods of amorphous alloy motors to simultaneously reduce their core and copper losses, and improve their comprehensive performances.

This paper provides the performance optimization and experimental validation of amorphous alloy high-speed asynchronous motors. Taking a 2.2 kW motor as an example, the finite element method (FEM) is used to compare its performances in the cases using amorphous alloy and silicon steel as the stator core materials, respectively. After deriving the optimization objectives of the amorphous alloy asynchronous motor, an evolutionary algorithm is used to optimize the geometrical parameters of its stator and rotor, so as to simultaneously reduce the core and copper losses whereas guaranteeing the desirable torque. The optimization results are validated through experiments, and the performance variation over a wide range of output torque and operational speed in different kinds of motors are investigated. Section II presents the modeling and simulation of high-speed asynchronous motors with different core materials. Section III introduces the optimization method and provides the optimization results. The related mechanisms are discussed. Section IV presents the motor prototype and the experimental validation results. Section V gives the key conclusions.

II. MODELING AND SIMULATION

A. MOTOR MODELS AND MATERIAL

The motor presented in this paper is a high-speed asynchronous motor for industrial fan drive motors. This

TABLE 1. High-speed three-phase asynchronous motor parameters.

Items	Value	Items	Value
Rated power P/kW	1.1	Rated voltage V	380
Rated speed n/rpm	7000	Number of poles	4
Outer diameter of stator D_{so}/mm	84.5	Outer diameter of rotor D_{ro}/mm	47
Inner diameter of stator D_{si}/mm	48	Inner diameter of rotor D_{ri}/mm	15
Number of stator slots	24	Number of rotor slots	34
Length of stator l/mm	80	Bar conductor type	copper
Number of per slot	40	Number of strands	1
Winding layers	1	Winding Connection	Y-connection
Material of the stator	35H300	Material of the rotor	35H300

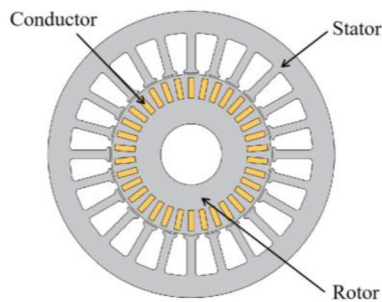


FIGURE 1. 2D model of the motor.

air-cooled motor has a rated power of 1.1 kW and a rated speed of 7000 rpm. Note that the stator core of this motor is made of silicon steel (35H300). The main structural parameters of this high-speed induction motor are shown in Table 1, and a two-dimensional finite-element model has been built in the Maxwell 2D Design platform as shown in Fig. 1. Note that the conductors shown in Fig. 1 cover the slots.

With the proposed FEM model of motor, the important material and structural properties should be considered and calculated. One of the important properties is the core losses of motor including hysteresis loss and eddy current loss, which depend on the size and material of the core. The core losses per unit volume can be expressed by [31]:

$$W_V = W_{Vh} + W_{Vc} + W_{Ve} \quad (1)$$

where W_{Vh} represents the hysteresis loss per unit volume. W_{Vc} represents the eddy current loss per unit volume. W_{Ve} represents the excess loss, accounting for a small proportion of the total loss. To reduce the stator core losses of motor, it is necessary to reduce these two important kinds of losses of W_{Vh} and W_{Vc} . Specifically, the hysteresis loss depends on the magnetostriction coefficient and the magnetic saturation induction strength, which can be expressed as:

$$W_{Vh} = C_h f B_m^2 \quad (2)$$

where C_h is the hysteresis loss factor, B_m is the core magnetic density and f is the operating frequency of the motor.

TABLE 2. Comparison of amorphous alloy 1K101-M and silicon steel 35H300 characteristics.

Performance indicators	1K101-M	35H300
Thickness (mm)	0.025	0.35
Minimum lamination factor	0.84	0.95
Resistivity ($\mu\Omega\cdot m$)	1.3	0.52
Saturation flux density (T)	1.63	2.03
Curie temperature ($^{\circ}C$)	399	750
Hysteresis factor (10^{-6} ppm)	27	8
Density (10^3 kg/m ³)	7.18	7.65

As for the eddy current loss W_{Vc} , it can be calculated as follows [9]:

$$W_{Vc} = \frac{\gamma}{6\rho} \pi^2 f^2 B_m^2 d^2 \quad (3)$$

where it can be observed that the eddy current loss W_{Vc} is proportional to the square of the thickness d of the material and inversely proportional to its resistivity ρ . γ is the electrical conductivity. By combining the above equations of Eqs. (2) and (3), it is clear that the use of materials with high resistivity and low thickness for motor cores can significantly reduce the core losses of the motor [32].

Therefore, in order to significantly reduce the core losses of the stator, the iron-based amorphous alloy (1K101-M) is used to replace the silicon steel as the material of the stator core of the above-mentioned high-speed asynchronous motor. Amorphous alloys can be formed by melting the iron, silicon, boron and other elements into the liquid based on a certain ratio between them, and then cooling them rapidly at a rate of more than one-million $^{\circ}C/s$, so as to ensure that the cooling rate can exceed the crystallization rate. It can be observed from Table 2 that 1K101-M has the superior magnetic conductivity and the higher resistivity, and its thickness is much lower than that of silicon steel sheet. These lead to the result that using the amorphous alloy as the material of the stator core can reduce the core loss.

B. SIMULATION AND ANALYSIS

Simulation is conducted by choosing 1K101-M and 35H300 as the stator core material of the amorphous alloy asynchronous motor (Motor-A) and the silicon steel asynchronous motor (Motor-S), respectively. Furthermore, the comparison between their simulation results is performed. The subsequent simulation processes are performed including pre-setting the model parameters, meshing the 2D model, finite element analysis and post-processing in the Ansoft software. In the case of the high-speed asynchronous motor with a rated output torque of 1.5 N·m and other parameters in Table 1, it is clearly observed from Fig. 2 that the core loss in the Motor-S is 26.62 W, while the core loss in the Motor-A is only 5.25 W. The core loss of the amorphous alloy asynchronous motor is 80.28% lower than that of the silicon steel asynchronous motor.

In addition to the core loss, copper loss is an important kind of losses in the motor as well, which increases with

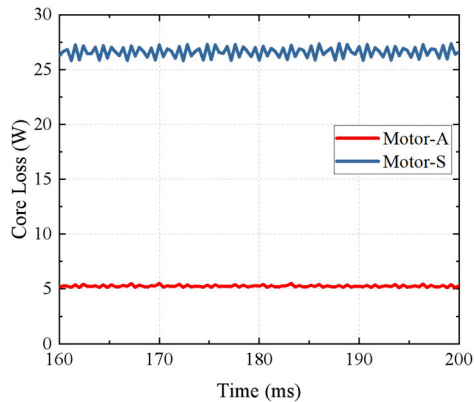


FIGURE 2. Core loss comparison between amorphous and silicon steel motors.

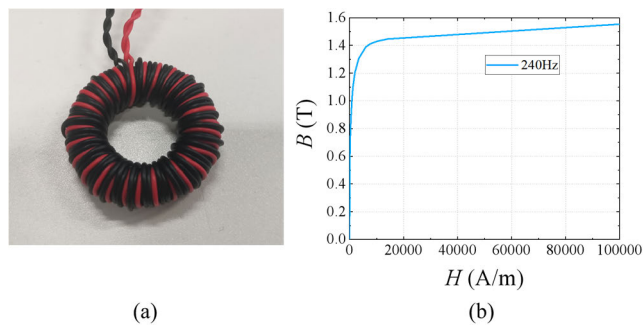


FIGURE 3. (a) 1K101-M with windings. (b) Magnetic density of 1K101-M test ring.

the increasing current in the conductor. For the amorphous alloy motor and the silicon steel motor with the same output torque, the excitation current of the amorphous alloy motor is higher. This is because that the saturation magnetic flux density of the amorphous alloy will drop significantly after the work procedures of lamination, paint dipping and curing, and cutting, etc. By testing the ring cores [33] of 1K101-M as shown in Fig. 3(a), it can be seen that the saturation magnetic density of the block drops below 1.6 at the operating frequency of 240 Hz as shown in Fig. 3(b).

When the magnetic flux density of the iron-based amorphous alloy (1K101-M) approaches the saturation value, its magnetic reluctance increases sharply. Due to this, if the magnetic flux should be further increased to increase the high torque, its stator current should be larger than that of the silicon steel motor. This, however, will lead to the increasing copper loss. The relations among the electromagnetic torque, the rotor bar currents and the magnetic flux under per pole can be expressed as follows:

$$T_e = C_t \phi_m I_2 \cos \varphi \quad (4)$$

where C_t is the torque constant, ϕ_m is the magnetic flux under per pole, $I_2 \cos \varphi$ is the active component of the rotor bar currents.

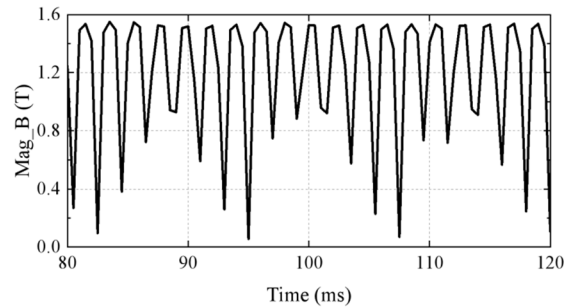


FIGURE 4. The magnetic flux (Mag_B) of the teeth.

It should be noted that the relationship between the electromagnetic torque T_e and the output torque T depends on the mechanical structure of motor, which can be expressed as:

$$T = T_e - T_m \quad (5)$$

where T_m is the mechanical torque loss. The mechanical torque loss can be divided into the friction loss and the inertia loss. Eq. (5) indicates that the mechanical torque loss T_m will decrease the practical output torque of the motor.

The FEM simulation is conducted to show the magnetic flux density of the Motor-A. For the rating torque of 1.5 N·m, the magnetic flux density of the stator teeth of the amorphous alloy high-speed asynchronous motor Motor-A is already as high as 1.53 T as shown in Fig. 4, which is close to its saturation magnetic flux density. The magnetic field strength is a key factor influencing the saturation magnetic flux density of the iron core. In the motor, the magnetic field strength depends on the current and coil design, and higher current and specific coil designs may result in increased magnetic field strength, subsequently affecting the saturation level of the iron core. Therefore, it can be known from the above discussions that with the same output torque, the Motor-A requires the higher current excitation than that of the Motor-S, which undoubtedly increases its copper loss. This is demonstrated via the FEM results as shown in Table 3. Compared with Motor-S, the maximum increasing percentage of copper loss of the Motor-A reaches 7.58% at the output torque of 0.5 N·m. Therefore, the traditional structural parameters of the silicon steel motor are not suitable for amorphous alloy motors. Specifically, the stator and rotor slots need to be redesigned to reduce the leakage flux and saturation density and enhance the air-gap flux. These can result in a reduction of the slippage rate and the current in the conductors of stator and rotor, leading to the reduction of the total copper losses of amorphous alloy asynchronous motors.

III. OPTIMIZATION AND ANALYSIS

A. OPTIMIZATION METHOD

The optimization problem of an amorphous alloy high-speed asynchronous motor includes multiple decision variables and multiple objective solutions that interact with each other, which cannot be simply expressed through the linear programming. Therefore, the optimization of the presented

TABLE 3. Comparison of copper loss between Motor-S and Motor-A.

Output Torque (N · m)	Motor-S Copper loss (W)	Motor-A Copper loss (W)	Percentage difference (%)
0.5	51.267	55.155	7.58
1	68.943	71.891	4.28
1.5	97.795	100.266	2.47
2	137.711	139.101	1.01
2.5	190.167	192.635	1.30
3	257.886	265.03	2.77

motor is a non-linear programming problem. The multi-objective non-linear programming problem can be mathematically described as follows [34]:

$$\begin{cases} \min y = F(x) = (f_1(x), f_2(x), \dots, f_m(x))^T \\ \text{s.t. } g_i(x) \leq 0; i = 1, 2, \dots, q \\ h_j(x) = 0; j = 1, 2, \dots, p \\ x \in X \end{cases} \quad (6)$$

where y is an m -dimensional target vector, the function $F(x)$ is called as the objective function, $g_i(x)$ and $h_j(x)$ are constraints, x is an n -dimensional decision vector, and the set X is an n -dimensional space vector.

When $x \in X$ and meet the constraints given, it can be considered as a feasible solution of the equation. All feasible solutions together are called the set of feasible solutions and denoted as X_f . The feasible solutions in which Pareto prevails among multiple feasible solutions will be combined into a new set, which is called the Pareto optimal solution set. The previous solutions for such nonlinear planning problems include directly deriving the analytical mathematical model. [35]. However, these methods lack the generality and simplicity, and require a great deal of preliminary work and knowledge in solving different problems. Moreover, the solutions are usually local optima rather than global optima over the whole parameter space. To solve these challenges, researchers have introduced the evolutionary algorithms to solve these problems. Early in 1985 Schaffer [36] proposed the evolutionary algorithm and implemented it for the first time in a multi-objective optimization problem.

With the advantages of strong search ability and better compatibility, the evolutionary algorithms can help find the global optimal solutions of multi-objective equations [37], [38]. Therefore, they can be introduced into the multi-objective optimization of amorphous alloy asynchronous motors. Evolutionary algorithms follow the principle of survival of the fittest in nature. The algorithm processes generally include the genetic coding, population initialization, crossover and mutation, selection and inheritance [39]. The population of the current generation is screened by setting a standard to obtain the better genes and pass them on to the next generation. Due to the principle of genetic variation, the problem of obtaining only locally optimal solutions can be solved. With the above advantages, multi-objective evolutionary algorithms are nowadays widely used in the design

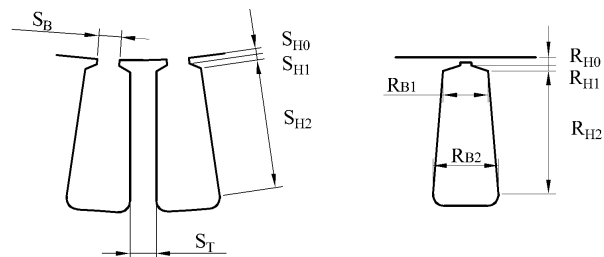


FIGURE 5. Stator slot shape (left) and rotor slot shape (right).

engineering. In the following section, the multi-objective evolutionary algorithm is applied to the structural optimization of amorphous alloy high-speed asynchronous motors.

B. RESULTS AND ANALYSIS

To improve the overall performance of amorphous asynchronous motors, the slot shapes of the stator and rotor should be optimized. Specifically, the dimensions of the slot opening height and slot shoulder height are small, and it is difficult to visualize the effect of their dimensional changes on the motor losses. Therefore, in order to improve the optimization efficiency and reliability, a multi-objective evolutionary algorithm is adopted to optimize the slot shapes of the stator and rotor. The structural parameters of slot to be optimized need to be selected before running the optimization program.

The different sizes of stator slot may affect the magnetic field distribution in the stator teeth and yoke. This may, result in the varying air gap permeability, leading to the change of excitation current. In addition, the peak value of the magnetic density in the stator may change and influence the motor losses, which in turn affects the motor efficiency. To reduce the undesirable variation in the air gap magnetic density caused by the slot opening width, a square semi-open slot is chosen for the stator design. To ensure the uniform magnetic density, a parallel teeth structure of stator is used with a variable width S_T . Due to the reason that the teeth width directly affects the slot fill rate, an upper limit is set for S_T . Furthermore, changing the teeth width directly affects the stator slot width. If the slot width is too small, the magnetic flux density and the losses will increase. Therefore, a lower limit is set for S_T as well. Besides S_T , the dimensional variables selected for the optimization of the stator slot include S_B , S_{H0} , S_{H1} , which are shown in Fig 5.

The important part of the copper loss is from the conducting bars of the rotor. When there is alternating current in the conductor, the closer it is to the surface of the conductor, the greater the current density is. In other words, the current inside the conductor is low, resulting in the large resistance of conductor and the high power loss. This phenomenon is called as the skin effect. The shape of the rotor slot is shown in Fig. 5. By properly designing the shape of the rotor slot, the skin effect can be reduced. Therefore, it is necessary to optimize the slot shape of the rotor. The copper loss of the

TABLE 4. Design parameters and value range.

Design parameters		Lower limit/mm	Upper limit/mm
Stator	S_B	1.8	3
	S_{H0}	0.5	2
	S_{H1}	0.1	1
	S_T	2.4	2.85
Rotor	R_{B1}	1.5	4
	R_{B2}	0.5	1.2
	R_{H0}	0.3	0.7
	R_{H2}	7	10.5

rotor can be expressed as follows:

$$P_{CR} = \sum_{\Delta} \frac{L_{ef} S_{\Delta} J_{\Delta}^2}{\sigma} \quad (7)$$

where L_{ef} is the effective shaft length of the rotor; S_{Δ} is the unit area of the rotor conducting bar; J_{Δ} is the rotor conducting bar current density. σ is the rotor bars resistivity.

From Eq. (7), it can be known that the copper loss of rotor is closely related with the effective cross-sectional area and current density of conductor. Optimizing the shape of the rotor slot can make the current distribution inside the conductor more uniform, effectively reduce the losses in the squirrel cage of the motor rotor, thus achieving the higher total efficiency. Therefore, the dimensional variables selected for the optimization of the rotor slot shape are R_{B1} , R_{B2} , R_{H0} , R_{H2} . Since the rotor has an external diameter of only 47 mm, the appropriate upper and lower limits should be set for the variables R_{B1} and R_{B2} for the optimization to avoid the conducting bars to overlap.

The above design parameters are introduced into the optimization evolutionary algorithm. After analyzing the relationship between the copper space factor and structural dimensions, their upper and lower limits are set as shown in Table 4.

For an asynchronous motor, its overall efficiency is closely related to the various losses of the motor, among which the mechanical loss P_{fw} is fixed with the motor structure unchanged, the stator winding copper loss P_{CS} and the rotor winding copper loss P_{CR} are influenced by the input and induced currents, and the core loss P_{Fe} is influenced by the stator material, provided that the overall size and rated working conditions are unchanged. Improving the efficiency of the motor indicates a reduction in the its losses, which can be known from in the following equations of total loss P and efficiency η :

$$\sum P = P_{CS} + P_{CR} + P_{Fe} + P_{fw} + P_S \quad (8)$$

$$\eta = \frac{P_1 - \sum P}{P_1} \quad (9)$$

where P_1 is the total input power of the motor.

Due to the fact that the saturation magnetic density of amorphous alloy is considerably lower than that of silicon steel, an inequality constraint should be added to the algorithm and the maximum magnetic density of the stator

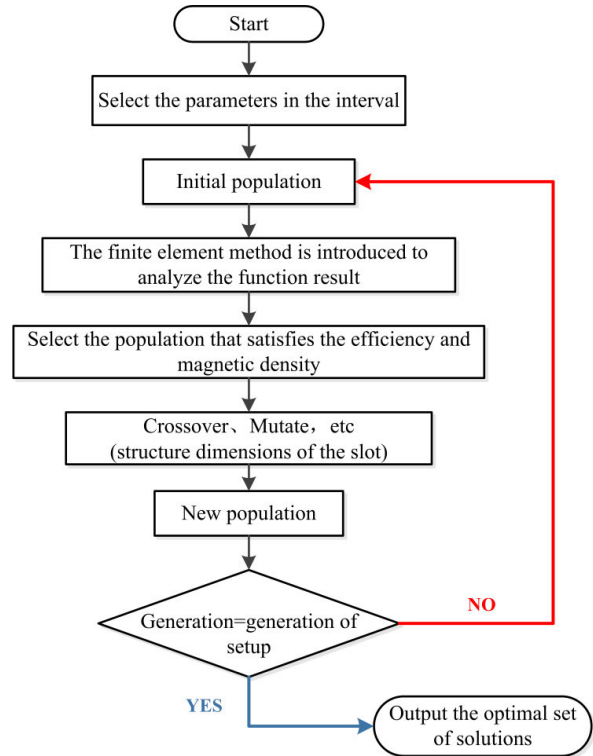


FIGURE 6. The flowchart of the evolutionary algorithm.

teeth should be less than 1.5 T. Furthermore, the output torque is set as one of the optimization objectives to ensure that the torque of the amorphous alloy asynchronous motors is comparable with that of the silicon steel ones. Therefore, the efficiency and output torque at rated power are set as dual optimization targets, which are both affected by the electrical density and magnetic density. With the chosen parameters and objectives, a multi-objective evolutionary algorithm approach is used to filter and iterate the parameters for the optimal results. The evolutionary algorithm is a global optimization method that can search more extensive parameter range compared with the traditional calculation method. Furthermore, it has the ability to learn and troubleshoot on its own, which greatly simplifies the traditional complex design process. The computational flow of the optimization program is shown in Fig. 6.

After the optimization simulation, the highest efficiency point is selected in the Pareto optimal data, which meets the torque requirements (1.5 N·m). The optimized design parameters are shown in the Table 5. The FEM model of the optimized motor is established as shown in Fig. 7, which is denoted as Motor-AO for distinction. The simulation of this FEM model is conducted to obtain the results of losses and efficiency. As shown in Fig. 8, it is clear that with the increasing output torque, the copper losses of both Motor-S and Motor-AO increase. Specifically, at a rated torque of 1.5 N·m, the amorphous alloy asynchronous motor Motor-AO has a copper loss of 82.99 W, which is decreased by 15.14% compared with that of the silicon steel motor Motor-S. This

TABLE 5. Optimized slot parameters.

Stator	Value/mm	Rotor	Value/mm
S_B	1.97191	R_{B1}	2.85767
S_{H0}	0.663929	R_{B2}	0.554532
S_{H1}	0.303724	R_{H0}	0.50
S_T	2.80	R_{H2}	8.58237

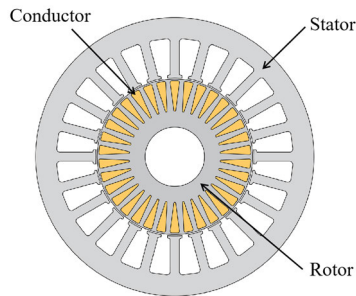


FIGURE 7. Model after optimization.

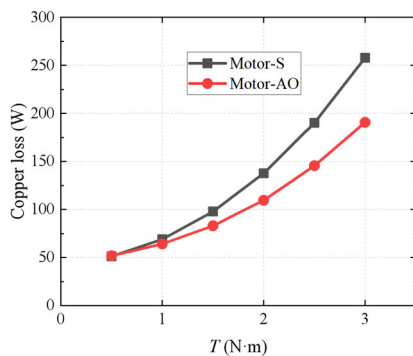


FIGURE 8. Comparison of copper losses in motors.

is due to the fact that the optimized shape of the rotor slot reduces the skin effect, leading to a reduction in the rotor harmonic currents and the copper loss. Overall, the “big on top, small on bottom” slot shape of the rotor is preferred in improving the motor efficiency.

The FEM simulation results of the indexes of the Motor-S, Motor-A and Motor-AO are shown in Table 6. It is clear that the optimization of the slot type shapes of both stator and rotor in Motor-AO reduces the operating current while ensuring the same output torque. Furthermore, the motor slip is reduced, leading to a further reduction of the total losses. Overall, compared with the Motor-S and Motor-A, the speed of constant operation of the Motor-AO is increased. Most importantly, the overall efficiency of the optimized amorphous asynchronous motor Motor-AO has been increased compared with the unoptimized one Motor-A and the silicon steel asynchronous motor Motor-S.

IV. EXPERIMENTAL VALIDATION

In order to validate the optimization results, the prototypes of Motor-A and Motor-AO were fabricated. The stator cores of both motors are made by the hot-pressing and WEDM (Wire

TABLE 6. Comparison of the performances of each motor at the rated operation.

Motor type	Efficiency $\eta/\%$	Torque $T/N \cdot m$	Total loss $\sum P/W$	Rated phase current I/A	Constant speed n/rpm
Motor-S	86.34	1.49	175.14	4.02	7064
Motor-A	88.57	1.49	142.9	4.09	7064
Motor-AO	90.42	1.49	117.13	3.88	7115

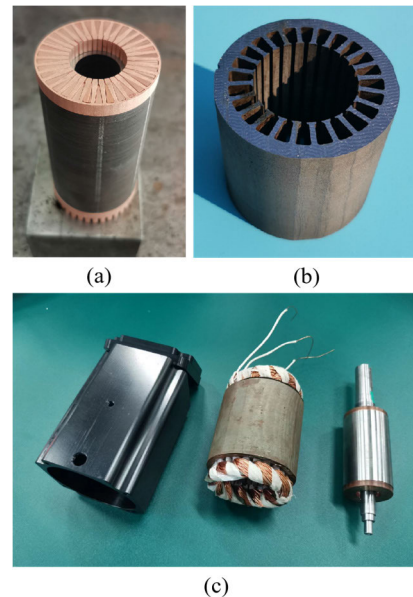


FIGURE 9. Cross sections and components of the prototype Motor-AO: (a) rotor, (b) stator and (c) components.

Electrical Discharge Machining) of amorphous alloy strips with the width of 142 mm. The silicon steel sheets used in the rotor are obtained by the stamping process. The cross sections of the rotor and stator of the motor Motor-AO are presented in Fig. 9(a) and (b), respectively. The disassembled prototype of the motor Motor-AO is shown in Fig. 9(c). The copper bars are linked together by the welding process, and the rotor core is filled with high-strength epoxy. The prototype of the silicon steel motor Motor-S is adopted from the products of YUSIN Co.

To verify the effectiveness of the optimization simulation, the original silicon steel motor Motor-S and the two amorphous alloy sample motors before and after optimization, Motor-A and Motor-AO, are tested respectively. An experimental platform is built to conduct the loading tests on the motors as shown in Fig. 10. A controller (NIDEC, UNIDRIVE M700) is used to drive the motor. The torque and speed of motor are measured by a sensor (DAYSENSOR, DYN-200), which are transmitted to a power analyzer (EVERFINE, PF3000M) for analysis.

The efficiency maps of the Motor-S, Motor-A and Motor-AO measured by the experimental platform are shown in Fig. 11-13, respectively. Comparing the three graphs, it can

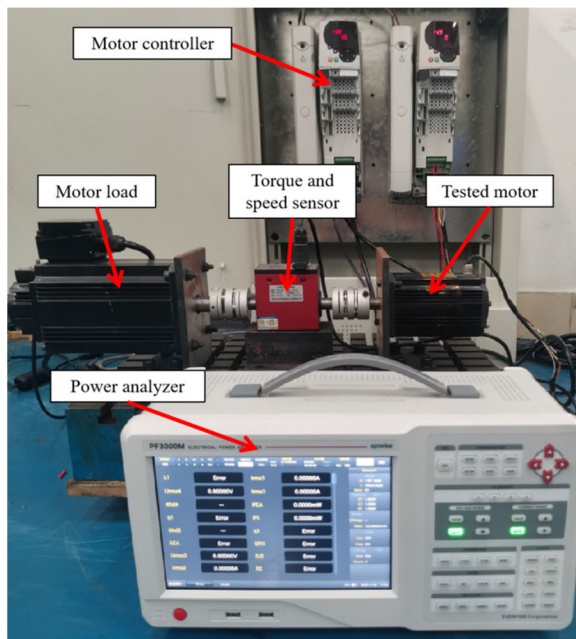


FIGURE 10. Experimental platform.

be seen that the highest efficiency of the motor Motor-AO is higher than the other two motors. Moreover, the high-efficiency (efficiency $\eta > 80\%$) range of output torque and operational speed of motor Motor-AO is the largest among all motors. In the range with high operational speed, for example 10000 r/min, the efficiency of the silicon steel motor Motor-S is significantly lower than those of the other two motors. This is mainly due to the higher iron loss of silicon steel compared with amorphous alloy at high frequencies. However, the high-efficiencies of Motor-A are concentrated in the range where the motor works at the high speed and the low output torque. In the other words, the motor Motor-A loses the high efficiency in the low-speed range. This disadvantage of the motor Motor-A is compensated in the motor Motor-AO. Furthermore, in the range of high torque ($T > 2.5 \text{ N}\cdot\text{m}$), the efficiency of the motor Motor-AO is significantly higher than that of the motor Motor-A. This is due to the fact that the optimized teeth slot shape reduces the magnetic density and the excitation current required to operate the motor.

A comparison of the efficiency of the motor running at different speeds with the same torque 1.5 N·m is clearly shown in Fig. 14. Specifically, at the operational speed of 7000 rpm, the efficiencies of Motor-S, Motor-A and Motor-AO are 84.5%, 86.8% and 90.5%, which are close to the optimization results. The efficiency of Motor-AO is increased by 4.29% and 7.12% compared with those of Motor-A and Motor-S, respectively. Overall, it can be concluded that the motor Motor-AO can improve the efficiency in the high-speed range while still maintaining relatively good performance in the low-speed range.

Besides the efficiency, the thermal behavior of the motor is of significance with respect to the motor life. Experiments

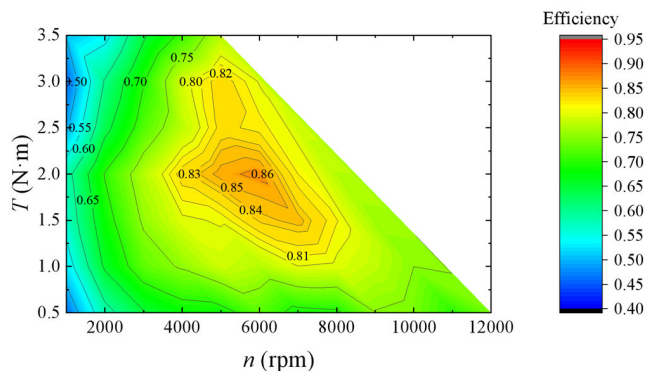


FIGURE 11. Efficiency map for Motor-S versus the output torque T and operational speed n.

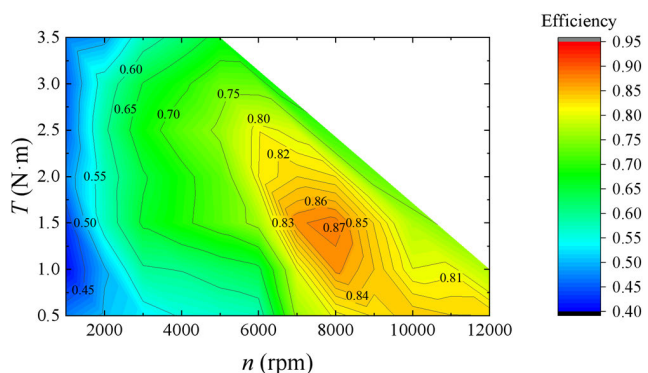


FIGURE 12. Efficiency map for Motor-A versus the output torque T and operational speed n.

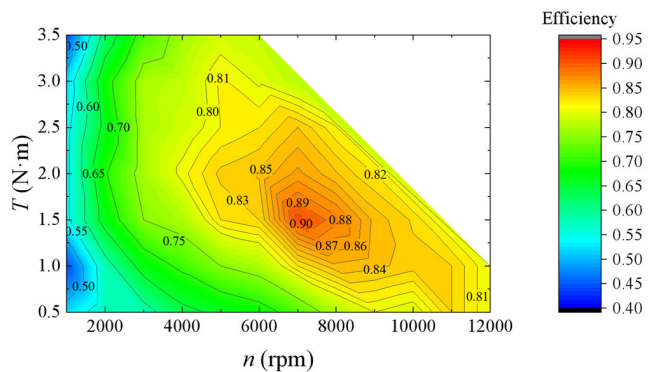


FIGURE 13. Efficiency map for Motor-AO versus the output torque T and operational speed n.

are conducted that three motors run for 10 minutes at the rated operational conditions of 1.5 N·m and 7000 rpm. Their temperature distribution is detected by an infrared detector (FOTRIC, 348X), results of which are shown in Figs. 15-17. The heat generation of the motor is reflected by checking the temperature of the motor case and the shaft exposed outside the rear end cover. It can be observed that the motor case temperature of the Motor-A is lower than that of the Motor-S. This is due to the fact that the amorphous alloy can effectively reduce the iron core losses of the stator. Despite this, the rotor

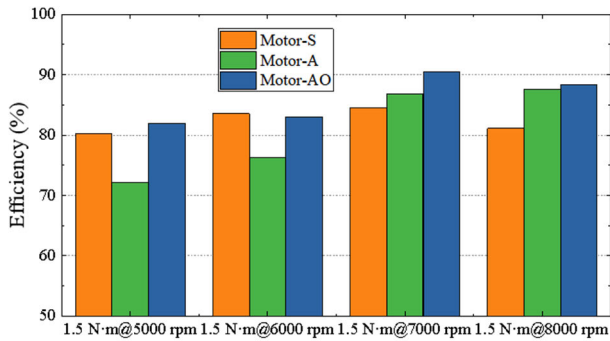


FIGURE 14. Comparison of the efficiencies of Motor-S, Motor-A and Motor-AO at different output torques and operational speeds.

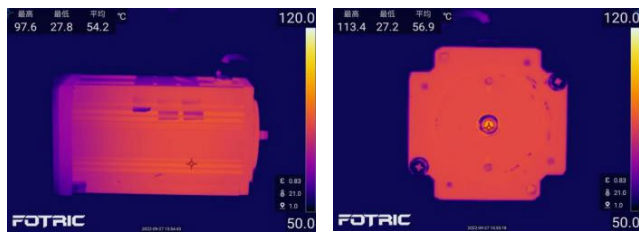


FIGURE 15. Thermal images of Motor-S motor case (left) and shaft (right).

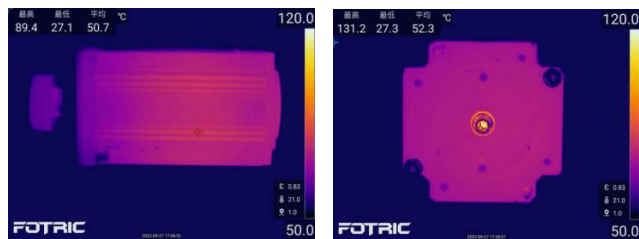


FIGURE 16. Thermal images of Motor-A motor case (left) and shaft (right).

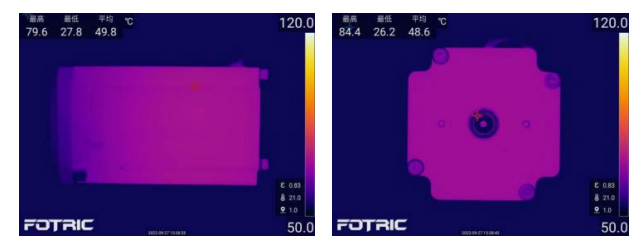


FIGURE 17. Thermal images of Motor-AO motor case (left) and shaft (right).

temperature of the Motor-A is increased compared with that of the Motor-S. Compared with the Motor-A and the Motor-S, the temperature of the case and rotor of the Motor-AO is significantly reduced simultaneously. The above discussions lead to the conclusion that the direct replacement of the stator core material, silicon steel to be the amorphous alloy will reduce the core loss whereas bring other problems such as the higher copper loss and the rotor overheat. These problems can be solved via the optimization of the rotor and stator slot shapes with the evolutionary algorithm.

V. CONCLUSION

Amorphous alloy has been used to replace the silicon steel as the stator core material of asynchronous motors for the core loss reduction under high-frequency operational conditions. However, due to its relatively low saturation magnetic density, this will bring the higher copper loss at the same time. Therefore, this paper proposes the evolutionary algorithm to optimize the stator and rotor shapes of the amorphous alloy asynchronous motor, so as to simultaneously reduce its core and copper losses. The finite element simulation of the silicon steel asynchronous motor and the amorphous alloy asynchronous motor before the optimization is conducted and compared. Based on the operational characteristic of motor, the output torque and the efficiency are set as dual optimization objectives. The constraints and variables in the evolutionary algorithm are set according to the properties of the material. With these settings, the slot shapes of stator and rotor are optimized, and it is found that the “big on top, small on bottom” slot shape of the rotor is preferred in improving the motor efficiency. Three motor models of Motor-S, Motor-A and Motor-AO are fabricated by machining and assembling, and their efficiencies are tested. Experimental results validate the optimization results and show that relatively low efficiency in the low-speed range of Motor-A is compensated in Motor-AO. Motor-AO possesses the largest high-efficiency range of output torque and operational speed. Specifically, at 1.5 N·m and 7000 rpm, the efficiency of Motor-AO can be improved by 4.29% and 7.12% compared with those of Motor-A and Motor-S, respectively.

REFERENCES

- [1] N. Ahmad, F. Khan, H. Ali, S. Ishaq, and E. Sulaiman, “Outer rotor wound field flux switching machine for in-wheel direct drive application,” *IET Electric Power Appl.*, vol. 13, no. 6, pp. 757–765, Apr. 2019.
- [2] Z. Wang, T. W. Ching, S. Huang, H. Wang, and T. Xu, “Challenges faced by electric vehicle motors and their solutions,” *IEEE Access*, vol. 9, pp. 5228–5249, 2021.
- [3] K.-Y. Hwang and B.-I. Kwon, “Design of low-cost BLAC motors for integrated electric brake systems,” *IEEE Access*, vol. 7, pp. 184183–184193, 2019.
- [4] A. Matsuoka, M. Sumino, S. Ueno, and T. Takeda, “Development of a high-speed motor at extremely low temperatures with an axial self-bearing motor and a superconducting magnetic bearing,” *Int. J. Appl. Electromagn. Mech.*, vol. 45, nos. 1–4, pp. 859–865, May 2014.
- [5] L. Shao, A. E. H. Karci, D. Tavernini, A. Sorniotti, and M. Cheng, “Design approaches and control strategies for energy-efficient electric machines for electric vehicles—A review,” *IEEE Access*, vol. 8, pp. 116900–116913, 2020.
- [6] A. Tikadar, J. W. Kim, Y. Joshi, and S. Kumar, “Flow-assisted evaporative cooling for electric motor,” *IEEE Trans. Transport. Electrification*, vol. 8, no. 1, pp. 1128–1143, Mar. 2022.
- [7] Z. Fan, H. Yi, J. Xu, K. Xie, Y. Qi, S. Ren, and H. Wang, “Performance study and optimization design of high-speed amorphous alloy induction motor,” *Energies*, vol. 14, no. 9, p. 2468, Apr. 2021.
- [8] H. Apaydin, O. Kara, and N. F. O. Serteller, “Investigation of the efficiency improvement on a 1.1 kW three-phase asynchronous motor,” *Turkish J. Electromechanics Energy*, vol. 7, no. 2, pp. 58–66, Oct. 2022.
- [9] Y. Liang, F. Zhao, K. Xu, W. Wang, J. Liu, and P. Yang, “Analysis of copper loss of permanent magnet synchronous motor with formed transposition winding,” *IEEE Access*, vol. 9, pp. 101105–101114, 2021.

- [10] C. Gan, J. Wu, Q. Sun, W. Kong, H. Li, and Y. Hu, "A review on machine topologies and control techniques for low-noise switched reluctance motors in electric vehicle applications," *IEEE Access*, vol. 6, pp. 31430–31443, 2018.
- [11] A. Makino, T. Kubota, K. Yubuta, A. Inoue, A. Urata, H. Matsumoto, and S. Yoshida, "Low core losses and magnetic properties of $\text{Fe}_{85-86}\text{Si}_{1-2}\text{B}_8\text{P}_4\text{Cu}_1$ nanocrystalline alloys with high B for power applications (invited)," *J. Appl. Phys.*, vol. 109, no. 7, Apr. 2011.
- [12] C. Li, F.-C. Huang, and Y.-Q. Wang, "An applicable real-time thermal model for temperature prediction of permanent magnet synchronous motor," *Proc. Inst. Mech. Eng., I, J. Syst. Control Eng.*, vol. 231, no. 1, pp. 43–51, Jan. 2017.
- [13] A. Shawier, A. S. Abdel-Khalik, R. A. Hamdy, K. H. Ahmed, and S. Ahmed, "Postfault operation of five-phase induction machine with minimum total losses under single open-phase fault," *IEEE Access*, vol. 8, pp. 208696–208706, 2020.
- [14] R. Sundaria, A. Lehtikoinen, A. Arkkio, and A. Belahcen, "Effects of manufacturing processes on core losses of electrical machines," *IEEE Trans. Energy Convers.*, vol. 36, no. 1, pp. 197–206, Mar. 2021.
- [15] Y. Hu, S. Zhu, L. Xu, and B. Jiang, "Reduction of torque ripple and rotor eddy current losses by closed slots design in a high-speed PMSM for EHA applications," *IEEE Trans. Magn.*, vol. 58, no. 2, pp. 1–6, Feb. 2022.
- [16] M. R. Jahangiri, H. Bayani, M. Ardestani, and M. Mehdizadeh, "Core loss reduction in grain oriented silicon steel sheets by two-sided laser scribing in the presence of a magnetic field," *J. Alloys Compounds*, vol. 891, Jan. 2022, Art. no. 162080.
- [17] L. Johnson, E. Cornell, D. Bailey, and S. Hegyi, "Application of low loss amorphous metals in motors and transformers," *IEEE Trans. Power App. Syst.*, vol. PAS-101, no. 7, pp. 2109–2114, Jul. 1982.
- [18] M. Dems and K. Komez, "Performance characteristics of a high-speed energy-saving induction motor with an amorphous stator core," *IEEE Trans. Ind. Electron.*, vol. 61, no. 6, pp. 3046–3055, Jun. 2014.
- [19] A. Chiba, H. Hayashi, K. Nakamura, S. Ito, K. Tungpimolrut, T. Fukao, M. A. Rahman, and M. Yoshida, "Test results of an SRM made from a layered block of heat-treated amorphous alloys," *IEEE Trans. Ind. Appl.*, vol. 44, no. 3, pp. 699–706, May/June. 2008.
- [20] M. Dems, Z. Gmyrek, and K. Komez, "Analytical model of an induction motor taking into account the punching process influence on the material properties' change of lamination," *Energies*, vol. 14, no. 9, p. 2459, Apr. 2021.
- [21] T. Kubota, A. Makino, and A. Inoue, "Low core loss of $\text{Fe}_{85}\text{Si}_2\text{B}_8\text{P}_4\text{Cu}_1$ nanocrystalline alloys with high bs and B800," *J. Alloys Compounds*, vol. 509, pp. 416–419, Jun. 2011.
- [22] S. Palko, *Structural Optimisation of an induction Motor Using a Genetic Algorithm and a Finite Element Method*. Helsinki Univ. Technology, 1996.
- [23] W. Jazdzynski, "Multicriterial optimisation of squirrel-cage induction motor design," *IEE Proc. B*, vol. 136, no. 6, pp. 299–307, Nov. 1989.
- [24] N. H. Fetih and H. M. El-Shewy, "Induction motor optimum design, including active power loss effect," *IEEE Trans. Energy Convers.*, vol. EC-1, no. 3, pp. 155–160, Sep. 1986.
- [25] G. Liuzzi, S. Lucidi, F. Parasiliti, and M. Villani, "Multiobjective optimization techniques for the design of induction motors," *IEEE Trans. Magn.*, vol. 39, no. 3, pp. 1261–1264, May 2003.
- [26] W. Yang, C. Huang, and Q. Zhang, "Optimization of squirrel-cage rotor for amorphous asynchronous motor," in *Proc. Chin. Automat. Congr.*, 2019, pp. 2107–2110.
- [27] A. Lei, C.-X. Song, Y.-L. Lei, and Y. Fu, "Design optimization of vehicle asynchronous motors based on fractional harmonic response analysis," *Mech. Sci.*, vol. 12, no. 1, pp. 689–700, Jul. 2021.
- [28] C.-H. Lin, "Altered grey wolf optimization and Taguchi method with FEA for six-phase copper squirrel cage rotor induction motor design," *Energies*, vol. 13, no. 9, p. 2282, May 2020.
- [29] M. Çunkaş, "Intelligent design of induction motors by multiobjective fuzzy genetic algorithm," *J. Intell. Manuf.*, vol. 21, no. 4, pp. 393–402, Aug. 2010.
- [30] T. Fan, Q. Li, and X. Wen, "Development of a high power density motor made of amorphous alloy cores," *IEEE Trans. Ind. Electron.*, vol. 61, no. 9, pp. 4510–4518, Sep. 2014.
- [31] Q. Zhang, J. Deng, and N. Fu, "Minimum copper loss direct torque control of brushless DC motor drive in electric and hybrid electric vehicles," *IEEE Access*, vol. 7, pp. 113264–113271, 2019.
- [32] B. Lingyun, Z. Zhengming, L. Yi, and W. Shuping, "Study on the loss reduction of high-efficient high-voltage series induction motors," in *Proc. Int. Conf. Electr. Mach. Syst.*, Aug. 2011, pp. 1–8.
- [33] G. Bramerdorfer and D. Andessner, "Accurate and easy-to-obtain iron loss model for electric machine design," *IEEE Trans. Ind. Electron.*, vol. 64, no. 3, pp. 2530–2537, Mar. 2017.
- [34] D. Griffel, "Multi-objective optimization using evolutionary algorithms," *Math. Gazette*, vol. 87, no. 509, pp. 409–410, Aug. 2003.
- [35] A. E. Eiben and J. Smith, "From evolutionary computation to the evolution of things," *Nature*, vol. 521, no. 7553, pp. 476–482, May 2015.
- [36] J. D. Schaffer, "Multiple objective optimization with vector evaluated genetic algorithms," Ph.D. dissertation, Dept. Elect. Eng., Vanderbilt Univ, Nashville, TN, USA, 1985.
- [37] K. Ramakrishnan, S. Stipetic, M. Gobbi, and G. Mastinu, "Optimal sizing of traction motors using scalable electric machine model," *IEEE Trans. Transport. Electrific.*, vol. 4, no. 1, pp. 314–321, Mar. 2018.
- [38] D. W. Zheng, M. Gen, and K. Ida, "Evolution program for nonlinear goal programming," *Comput. Ind. Eng.*, vol. 31, nos. 3–4, pp. 907–911, Dec. 1996.
- [39] C. T. Krasopoulos, I. P. Armouti, and A. G. Kladas, "Hybrid multiobjective optimization algorithm for PM motor design," *IEEE Trans. Magn.*, vol. 53, no. 6, pp. 1–4, Jun. 2017.



JIAHAO ZHANG (Member, IEEE) received the B.S. degree in vehicle engineering from the School of Rail Transportation, Wuyi University, Jiangmen, China, in 2020. He is currently pursuing the master's degree in mechanical engineering with Shenzhen University, Shenzhen, China. His current research interests include amorphous alloy motors and transformers, high-speed electric motors, and wind generators.



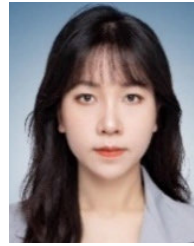
RONGGAO CUI received the Ph.D. degree in mechanical engineering from Shanghai Jiao Tong University, Shanghai, China, in 2021. He is currently an Engineer with the Department of Motor Design Business, Weichai New Energy Technology Company Ltd., Weifang, China. His current research interests include the design of electric motors for new energy vehicles and transformers.



YU WEI received the M.S. degree in rail transit engineering from Shenzhen University, Shenzhen, China, in 2016. He is currently a Research Assistant with the College of Mechatronics and Control Engineering, Shenzhen University. His current research interests include amorphous alloy motors and transformers, high-speed electric motors, and wind generators.



DEGUI YU received the M.S. degree in mechanical engineering from Shenzhen University, Shenzhen, China, in 2009. He is currently a Laboratory Technician with the College of Mechatronics and Control Engineering, Shenzhen University, China. His current research interests include the design and control of high-speed electric vehicle motors, technologies of power electronics, microcontrollers, and embedded systems.



SHITONG FANG received the B.S. degree in mechanical engineering from Sun Yat-sen University, Guangzhou, China, in 2017, and the Ph.D. degree in mechanical engineering from The Chinese University of Hong Kong, Hong Kong, China, in 2021. She is currently an Assistant Professor with the College of Mechatronics and Control Engineering, Shenzhen University, China. Her current research interests include amorphous alloy motors and transformers, energy generators, and nonlinear system modeling.



SHUNDE XIE received the M.S. degree in mechanical engineering from Shenzhen University, Shenzhen, China, in 2021. He is currently a Research Assistant with the College of Mechatronics and Control Engineering, Shenzhen University. His current research interests include amorphous alloy motors and transformers, high-speed electric motors, and wind generators.



JUN SHEN was with the Harbin Institute of Technology, from 1993 to 2011, where he became a Professor, in 1999. From 2003 to 2005, he was a Visiting Scholar with The University of Sydney and the University of Nottingham. He was a Professor with Tongji University, from 2011 to 2018. Later, he joined Shenzhen University as a Distinguished Professor. His current research interests include the fabrication and application of metallic glasses, the high-efficient amorphous alloy electric motors, wind generators, and transformers.

...